ENVIRONMENTAL RESEARCH
LETTERS

LETTER • OPEN ACCESS

The difference in the uncertainty sources between future projections of mean and extreme precipitation over East Asia

To cite this article: Ana Juzbašić *et al* 2024 *Environ. Res. Lett.* **19** 074015

View the article online for updates and enhancements.

You may also like

- Intensification of summer precipitation with shorter time-scales in Europe
Ø Hodnebrog, L Marelle, K Alterskjær et al.
- Diverse estimates of annual maxima daily precipitation in 22 state-of-the-art quasi-global land observation datasets
Margot Bador, Lisa V Alexander, Steefan Contractor et al.
- Attributing observed increase in extreme precipitation in China to human influence
Siyan Dong, Ying Sun and Xuebin Zhang

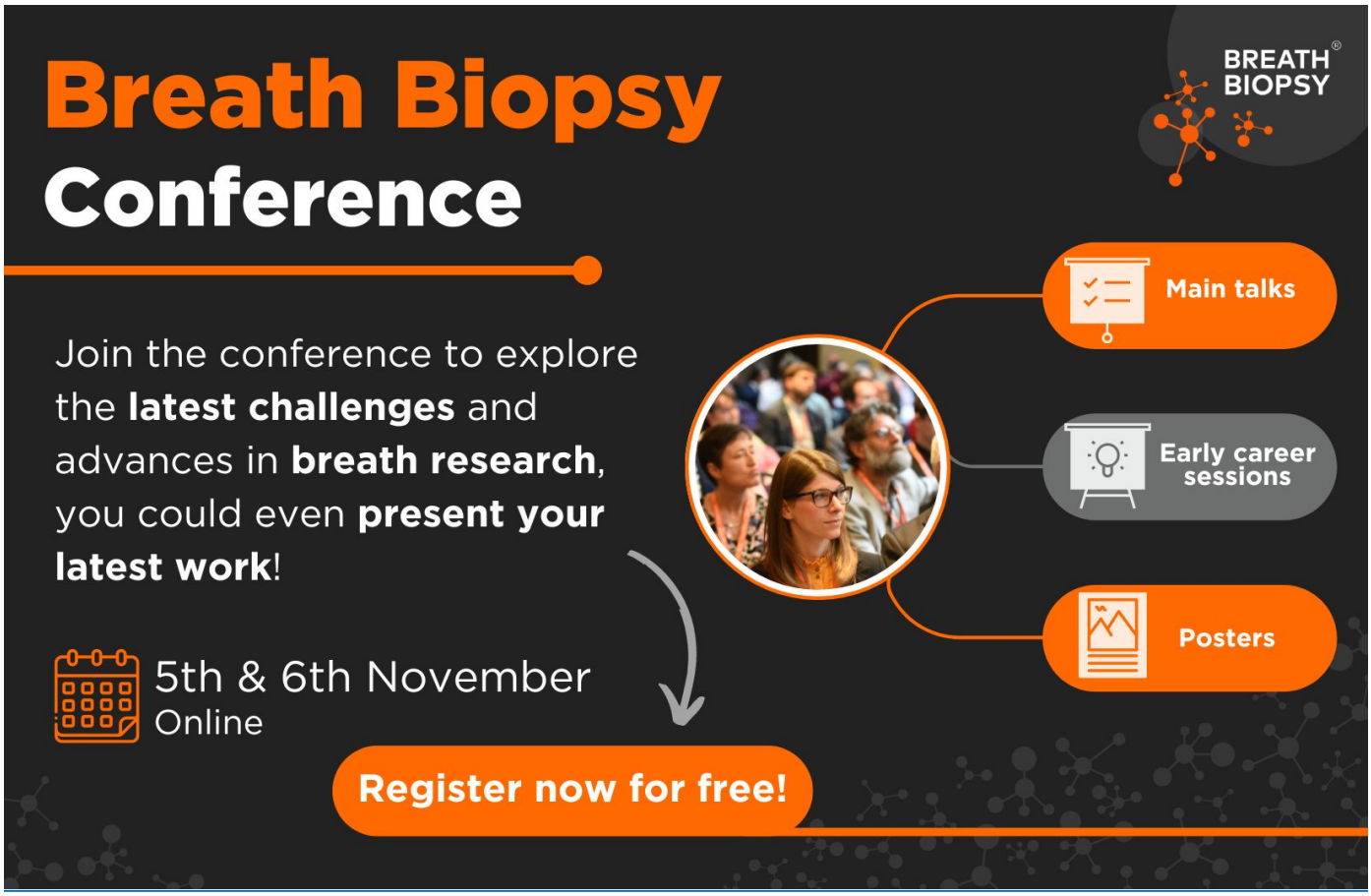

This content was downloaded from IP address 114.70.7.203 on 11/07/2024 at 07:41

ENVIRONMENTAL RESEARCH
LETTERS

LETTER

The difference in the uncertainty sources between future projections of mean and extreme precipitation over East Asia

Ana Juzbašić[1], Changyong Park[1,*], Dong-Hyun Cha[1,*], Joong-Bae Ahn[2], Eun-Chul Chang[3], Seung-Ki Min[4], Youngeun Choi[5] and Young-Hwa Byun[6]

[1] Department of Civil, Urban, Earth and Environmental Engineering, Ulsan National Institute of Science and Technology, Ulsan, Republic of Korea
[2] Department of Atmospheric Sciences, Pusan National University, Busan, Republic of Korea
[3] Department of Atmospheric Science, Kongju National University, Kongju, Republic of Korea
[4] Division of Environmental Science and Engineering, Pohang University of Science and Technology, Pohang, Republic of Korea
[5] Department of Geography, Konkuk University, Seoul, Republic of Korea
[6] National Institute of Meteorological Sciences, Seogwipo, Republic of Korea
[*] Authors to whom any correspondence should be addressed.

E-mail: parkcy@unist.ac.kr and dhcha@unist.ac.kr

Keywords: extreme precipitation, uncertainty, future projection, regional climate model, East Asia

Supplementary material for this article is available online

OPEN ACCESS

RECEIVED
3 February 2024

REVISED
15 May 2024

ACCEPTED FOR PUBLICATION
31 May 2024

PUBLISHED
13 June 2024

Original content from this work may be used under the terms of the Creative Commons Attribution 4.0 licence.

Any further distribution of this work must maintain attribution to the author(s) and the title of the work, journal citation and DOI.

Abstract

As the incidence of extreme precipitation events attributable to global climate change increases, providing policymakers with accurate model predictions is of the utmost importance. However, model projections have inherent uncertainties. The present study attempted to distinguish the sources of the uncertainty of the mean and extreme precipitation projections in the East Asia region using the mean boreal summer precipitation, simple precipitation intensity index (SDII), maximum cumulative 5 day precipitation, and annual maximum daily precipitation (Rx1d). The results show that while the mean precipitation was projected to change very little regardless of the scenario, more extreme indices were projected to increase considerably by the end of the century, particularly in the high-emissions scenarios. On average, model uncertainty accounted for the largest part of the uncertainty. However, for Rx1d in the 2030s, as well as mean and SDII in some regions until the 2060s, the internal variability was the largest contributor. In addition, whilst scenario uncertainty accounted for a negligible proportion of average precipitation variability, for the more extreme the precipitation indices, scenario uncertainty contribution to total variability by the end of the century was significant; namely, the scenario uncertainty contribution was overall highest for the maximum one-day precipitation. Additionally, comparatively wetter regions had greater overall projection uncertainties, especially uncertainty arising from internal variability, likely due to the influence of interannual variability from the EA summer monsoon.

1. Introduction

The incidence of precipitation extremes is increasing worldwide (IPCC 2014, 2022). Heavy precipitation intensification, increased tropical cyclone landfall risk, and associated flooding, along with intensified droughts projected in the future, are likely to cause involuntary migration of people in the mid-to-long-term (IPCC 2022). East Asia (EA) is especially vulnerable to climate change owing to the combination of high population density living near coastlines as well as natural and topographic factors (IPCC 2014, 2022). Therefore, owing to the potential damage caused by extreme precipitation events, it is imperative to provide policymakers with accurate and reliable climate projections over the EA. However, climate projections by climate models depend on a number of factors, such as different emissions and radiative forcing, as well as various model settings and parametrizations, resulting in a wide range of plausible future scenarios, leading to certain levels of uncertainty in any projection (Flato *et al* 2013, Vial *et al* 2013, Lee *et al* 2021). Several sources contribute to uncertainty in future climate projections. Understanding in

© 2024 The Author(s). Published by IOP Publishing Ltd

detail how each source contributes to the total uncertainty in future climate projections can help us more effectively respond to climate change. Accordingly, many attempts have investigated the sources contributing to uncertainty in future climate projections. Two of the most common ways to separate uncertainty are the fit-to-polynomial (Hawkins and Sutton 2009, 2011), and the two-way analysis of variance approaches (Suzuki-Parker *et al* 2018, Christensen and Kjellström 2021, Lee *et al* 2023). The former focuses on separating the uncertainties arising from internal variability, models, and different emissions scenarios, whereas the latter focuses on separating the uncertainties originating from global climate models (GCMs) and regional climate models (RCMs).

There has been a large body of research regarding future climate change uncertainties on a global scale (Hawkins and Sutton 2009, Chen *et al* 2014, Lehner *et al* 2020); Europe (Rajczak *et al* 2013, Kutiel 2019); the North American region (Monier *et al* 2014), and EA (Park *et al* 2023). However, most of these studies focused on uncertainties in the mean annual or seasonal changes and were often performed using data obtained from GCMs. Because of this, understanding of the uncertainties in extreme precipitation event changes on smaller regional scales, specifically over the EA domain, remains limited.

Considering their coarse resolution, GCMs are insufficient for detailed future climate simulations on regional scales, especially in domains involving complex terrain and coastal regions (Gao *et al* 2006, Rummukainen 2015, Torma *et al* 2015, Kim *et al* 2020a). To resolve this issue, as well as to provide coordinated sets of regional projections worldwide, the World Climate Research Programme established the Coordinated Regional Climate Downscaling Experiment (CORDEX) project. The CORDEX EA project team has produced dynamically downscaled data using several RCMs forced by various GCMs, which have been used as the basis for numerous studies on the future climate (Park *et al* 2016, 2020, 2021, Lee *et al* 2017, Jo *et al* 2019, Juzbašić *et al* 2022, Kim *et al* 2023, Seo *et al* 2023).

Therefore, this study aimed to provide insights into the uncertainties regarding extreme precipitation projections over EA. This is the first study to separate the uncertainty sources for extreme precipitation projections over the EA using high-resolution datasets from multi-GCM and multi-RCM simulations. For policymaking, knowing the influence of the different sources of uncertainty, especially the amount of variability arising from the different emissions scenarios, is of paramount importance.

Table 1. Abbreviations and descriptions of the sub-regions used in this study.

Abbreviation	Geographical region
NEC	Northeastern China
NC	Northern China
YHR	Yangtze–Huaihe River Basin
SC	Southern China
KO	Korean Peninsula
JP	Japan

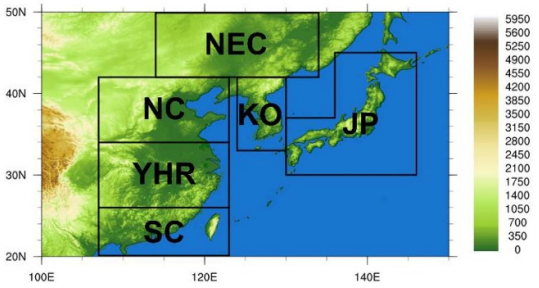

Figure 1. Elevation (unit: m) map of the domain with marked sub-regions described in table 1.

2. Data and methods

2.1. Datasets and domain

The EA domain analyzed in the present study (defined as the area between 100–150° E and 20–50° N) encompasses most regions vulnerable to changes in extreme precipitation, including parts of China, Korea, and Japan. The primary domain was divided into six sub-regions for a more detailed spatial analysis (table 1). The geographical locations and the topography of the sub-regions are shown in figure 1.

This study used daily precipitation data for the boreal summer period (June–July–August, JJA). The model data used in this study was produced as a part of the CORDEX-EA Phase II project. Fifteen different GCM–RCM chains were used, of which 10 used representative concentration pathway (RCP) scenarios, and five used shared socioeconomic pathway (SSP) scenarios for future projections. Only one realization of each model was used in the present study. Models using RCP scenarios are the three GCMs from the Coupled Model Intercomparison Project Phase 5 (CMIP5), namely the GFDL-ESM-2M (Geophysical Fluid Dynamics Laboratory Earth System Model, Zadeh *et al* 2012), HadGEM2-AO (Hadley Centre Global Environment Model version 2—Atmosphere–Ocean, Martin *et al* 2011), and Max Planck Institute ESM Low Resolution (MPI-ESM-LR) (Giorgetta *et al* 2013). The (UK-ESM (Sellar *et al* 2019) was selected from CMIP phase 6, which uses SSP scenarios. The GCMs selected in this study have been shown to

accurately simulate the East Asian climate (e.g. Seo *et al* 2013, Guo *et al* 2016). UKESM, which is built on he HadGEM3 model, has been selected as the representative of CMIP6 models for the 2nd phase of CORDEX-EA as it is a continuation of the HadGEM model series, which have been proven to simulate Asian Climate reasonably. The details of the six regional models used for downscaling in the present study, as well as all GCM–RCM chains, are listed in table 2.

The regional models in this phase of the CORDEX project were run on a 25 km curvilinear grid. Dynamical downscaling has been shown to have added value, especially in regions of complex terrain, and these specific models have been shown in previous studies to simulate the precipitation over EA adequately (e.g. Park *et al* 2016, Kim *et al* 2020b, Hui *et al* 2022, Kim *et al* 2022, Seo *et al* 2023). For easier comparison, the model data were regridded using bilinear interpolation to the common $0.25 \times 0.25^{\circ}$ grid. As the CMIP5 and CMIP6 historical experiments were conducted over slightly different periods, the common period from 1981–2005 was used as historical reference period. To evaluate future changes, two scenario combinations were used: RCP2.6 and SSP1-2.6, and RCP8.5 and SSP5-8.5. The future period analyzed in this study was 2015–2099, as the CMIP6 model future period began in 2015, and some of the models did not extend to 2100. The future period was divided into three time spans: the near future (2025–2049), mid-future (2050–2074), and distant future (2075–2099) for detailed analysis. As the forcing in the SSP scenarios follows the emissions assumed in the RCP scenarios, a direct comparison was considered appropriate. Li *et al* (2021) showed that corresponding scenario projections for the CMIP5 and CMIP6 models for EA showed similar changes for both mean and extreme precipitation. The aforementioned combinations were chosen as they represent the opposites—with RCP2.6/SSP1-2.6 being closest to the goal of the Paris Agreement, and the RCP8.5/SSP5-8.5 scenario being the projection assuming continuous heavy fossil fuel use, the so-called 'business as usual' scenario. In the present study, none of the RCMs are coupled with aerosol models, and the concentrations and levels of aerosols are kept at the climatological level within RCMs, meaning that the aerosol effects are only included through the indirect impact through the boundary conditions.

Because bias correcting the data can add additional uncertainties to the future projections (Lafferty and Sriver 2023), and for precipitation projections, the percentiles were used instead of raw values, the bias correction has not been performed in this study.

2.2. Methods

2.2.1. Extreme precipitation indices

The present study used four precipitation intensity indicators, defined by the Expert Team on Climate Change Detection and Indices (Klein Tank *et al* 2009): JJA mean precipitation; simple daily intensity index (SDII), which is the precipitation on rainy days (days with > 1 mm precipitation) divided by the number of rainy days; maximum daily precipitation (Rx1d); and maximum cumulative five-day precipitation (Rx5d). Each index was calculated at each grid point for each year, for each model separately. Only grid points located on land were used.

2.2.2. Separating the uncertainties

Uncertainties were decomposed according to the methodology described by Hawkins and Sutton (2009, 2011). Each grid point was analyzed separately. The total uncertainty of each projection consists of three parts: internal system variability, model uncertainty, and uncertainty arising from differences in forcing, known as scenario uncertainty. Internal variability of the system encompasses the factors arising from natural variability of the system, that happen in the absence of any radiative forcing. These fluctuations are an intrinsic feature of non-linear dynamic systems, and arise, among other things, from uneven distribution of energy across the globe. An example of such variability would be El Nino Southern Oscillation. Additionally, these uncertainties can also arise from the imperfect initializations of the system.

First, each model projection was fitted for the whole period from 1981 to 2099 using a least squares fit to a fourth-order polynomial. The raw projection is as follows.

$$X_{m,s,t} = x_{m,s,t} + i_{m,s} + \varepsilon_{m,s,t} \tag{1}$$

where x denotes the fit, i denotes the reference value, and the reference value used is the historical average. Finally, ε is the residual of the fit. The subscripts refer to model (m), scenario (s), and time (t), respectively, where time is in years.

The internal variability component is defined as the variance of the residuals of the fits:

$$\mathrm{IV} = \frac{1}{N_m} \sum_{m} \mathrm{var}_{s,t} \left(\varepsilon_{m,s,t} \right), \tag{2}$$

where N represents the number of models (15). This parameter does not change over time. In addition, the calculated internal variability value was slightly different for each model; therefore, a multi-model mean was used.

Model uncertainty was calculated as the multi-scenario mean of the variance of the different model

Table 2. Regional climate models used in this study, along with the forcing GCMs, parametrizations, and horizontal resolutions.

		RCM parametrizations						
RCM	CGCMs downscaled	CPS (convection parameterization schemes)	Microphysics	Radiation	LSM (land surface model)	PBL (planetary boundary layer)	Resolution (lat. x lon.), Number of grid points	RCM references
WRF v.4	GFDL-ESM2M MPI-ESM-LR UK-ESM	Betts–Miller–Janjic	WSM3	Community Atmospheric Model radiation scheme (CAM)	NOAH	Yonsei University (YSU) PBL	25 km, 250 × 395	(Gochis *et al* 2017)
RegCM v.4	GFDL-ESM2M, HadGEM2-AO UK-ESM	MIT–Emanuel	SUBEX	NCAR CCM3	NCAR CLM3.5	Holtslag	25 km, 249 × 394	(Giorgi *et al* 2012)
MM5 v.5	HadGEM2-AO MPI-ESM-LR	Kain and Fritsch	Reisner II	CCM2 radiative transfer scheme	CLM3	YSU	25 km, 260 × 405	(Grell *et al* 1994)
CCLM v.5	HadGEM2-AO MPI-ESM-LR UK-ESM	Tiedke	Extended DM	Ritter and Galeyn	TERRA ML	Davies and Tumer	25 km, 231 × 376	(Doms and Baldauf 2013)
HadGEM3-RA	HadGEM2-AO, MPI-ESM-LR, UK-ESM	Revised mass flux	Single moment bulk	General 2-stream radiation	Joint UK Land Environment Simulator (JULES)	Smith (1990), Lock *et al* (2000)	25 km, 251 × 396	(Davies *et al* 2005)
GRIMs	UK-ESM	Simplified Arakawa–Schubert	WSM1	LW: Chou, SW: Chou and Suarez	NOAH	YSU PBL	25 km, 252 × 401	(Hong *et al* 2013)

projection fits. This uncertainty arose from the different schemes and parameters used in the models, resulting in slightly different projections for the same radiative forcing.

$$\mathrm{MU}(t) = \frac{1}{N_s}\sum_{s}\mathrm{var}_m\left(x_{m,s,t}\right), \tag{3}$$

where N indicates the number of scenarios.

Finally, the multi-model mean variance was used as a scenario uncertainty (SU) parameter:

$$\mathrm{SU}(t) = \mathrm{var}_s\left(\frac{1}{N_m}\sum_{m}x_{m,s,t}\right). \tag{4}$$

These uncertainty components were assumed to be independent. Therefore, total variance (T) is the sum of the three components.

$$T(t) = \mathrm{IV} + \mathrm{MU}(t) + \mathrm{SU}(t). \tag{5}$$

3. Results

3.1. Future projections

The simulated changes in the extreme precipitation indices in EA for the three future periods are shown in figure 2. The area-averaged mean JJA precipitation was not projected to have significant changes in either scenario, with an increase of 5.5% and 12.8% by the end of the century in the low- and high-emissions scenarios, respectively. The SDII changes in all periods were projected to be somewhat larger than the mean precipitation in high-emissions simulations, but with a similar magnitude of change as the mean in the low emission scenarios. In contrast, Rx5d and Rx1d showed greater changes under higher emissions scenarios, continuously increasing until the end of the century. Specifically, Rx1d was projected to increase by 33% on average by the end of the century in the RCP8.5/SSP5-8.5, with certain parts of the domain exceeding a 50% increase. According to these results, in the high-emissions scenarios, the increase rate of the high-intensity extreme precipitation indices (e.g. Rx5d and Rx1d) is greater than the average precipitation and the low-intensity extreme precipitation index (e.g. SDII). Moreover, this is expected to increase further over time. Additionally, previous research (Samset *et al* 2019, Zhao *et al* 2019, Wilcox *et al* 2020) has shown that there is a non-negligible effect on precipitation from East Asian Summer monsoon due to the cloud-aerosol interactions, in a sense that decrease in aerosol emissions results in both higher warming, but also higher increases in extreme precipitation. However, as the present study uses just one run of all of the models, and RCMs do not directly simulate changes in aerosol concentrations, it would be hard to quantify these effects and separate them from the effects of greenhouse gas emissions. That is, the effects of aerosol changes are included in the RCM simulations through the indirect impacts of the boundary conditions, while the aerosol levels themselves are kept constant at climatological levels in the RCMs as they were set up for this study. The differences in the responses in different regions can also partially be accounted for by the future changes in EASM, namely changes in low-level vapor, as well as the changes in southerly winds, bringing more moisture to specific parts of the domain (Kim *et al* 2020a).

3.2. Uncertainties of future extreme precipitation projection

Figure 3 is a cascade plot showing the projected area-averaged percentages of change at the beginning, middle, and end of the century (top, middle, and bottom of the graph, respectively). This uncertainty cascade plot is an intuitive tool that easily identifies the contribution of uncertainty components (e.g. model spreads and scenario ranges) (Park *et al* 2023). The top point of each cascade plot is the average estimated change from all models and scenarios, the middle points denote the average of each scenario (blue for lower emissions and red for higher emissions), and the bottom points are the projections of each separate model (Hawkins 2014, Swart *et al* 2015, Park *et al* 2023). Therefore, the larger the difference between the two points in the middle, the greater the scenario uncertainty, whereas the bottom points (model spread) denote the general model uncertainty. The spread between the models increases with time, with the 2090s having the widest and the 2030s having the narrowest spread. Overall, the spread between the models for the same emission scenario is lowest for SDII, but the spread between the different emission projections is lowest for the mean precipitation for all the periods and all sub-regions except NEC, where SDII and Rx5d have very small spread between different projections in the 2060s. There are very minor differences, if any, between different warming scenarios for the projections of mean precipitation in the 2030s and 2060s for all regions between NEC and YHR. At the end of the century, the spread between the scenarios is, for all sub-regions, largest for Rx1d, signifying that the most extreme precipitation is the most affected by anthropogenic changes. The spread between the models themselves is largest for the NEC domain for all the indices except Rx1d, where at the end of the century, the SC domain has the most extensive spread, especially in the high emission scenarios (marked in red). Additionally, in general, the

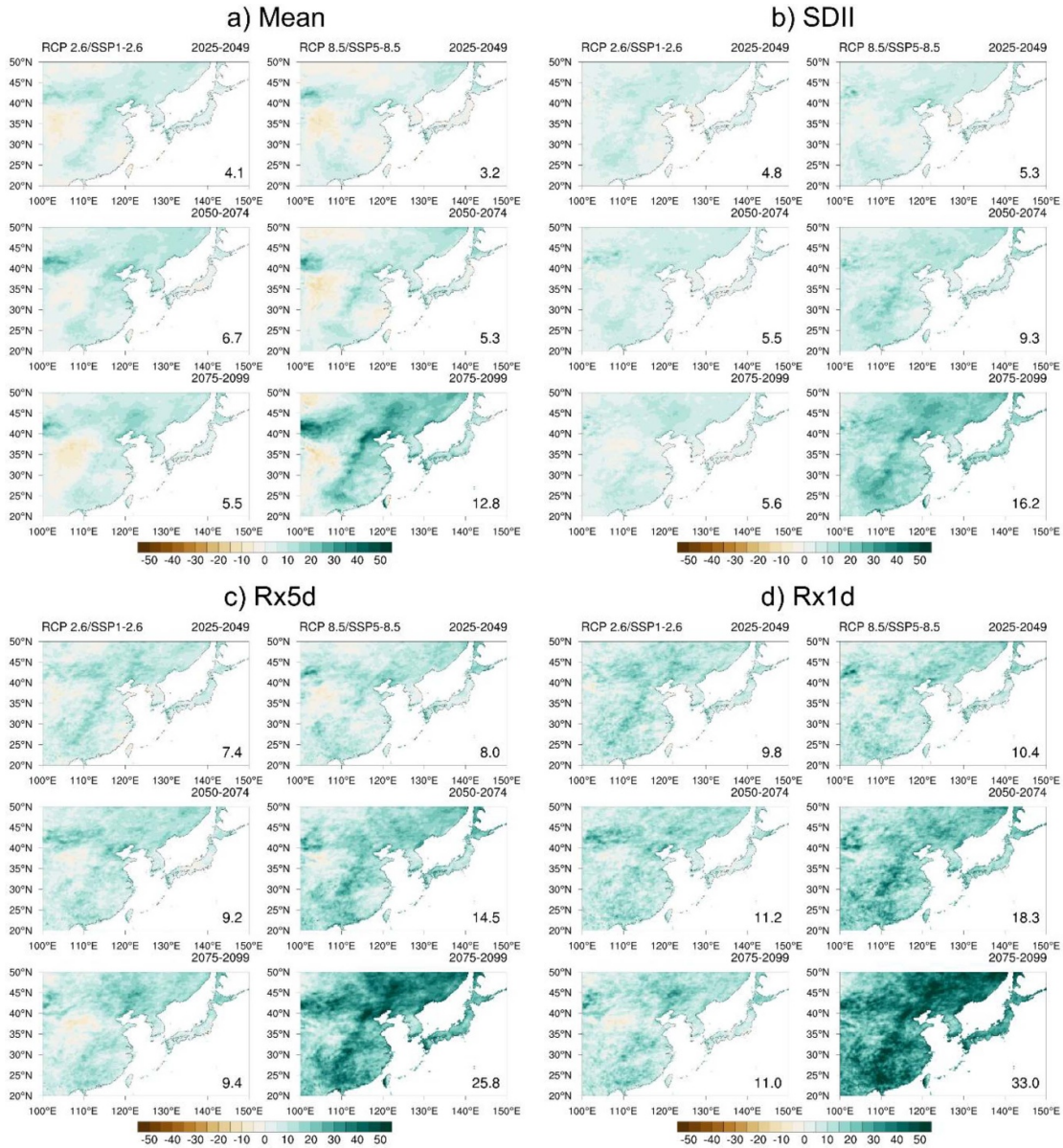

Figure 2. The changes (%) of the precipitation indices from least to most extreme: a) daily mean, b) SDII, c) Rx5d, and d) Rx1d. Area mean values are given in the bottom right corners.

model spread is wider for the higher emission scenarios than for the lower for all the indices, implying that higher emissions also lead to more model variability in the projections, which is likely a consequence of different climate sensitivities of the different models.

Figure 4 shows the contribution of each uncertainty component at different times in the future, namely in the 2030s, 2060s, and 2090s. To reduce noise, the fine resolution model data has been averaged per $1° \times 1°$. In the 2030s, for mean and SDII, depending on the area, either internal variability or the model uncertainty accounted for the majority of the variability. For Rx5d and Rx1d, however, internal variability component accounted for the majority of the variability over most of the domain. The scenario uncertainty contribution was negligible for all the indices. In the 2060s, model uncertainty was the primary source of uncertainty for all indices. This is particularly notable for mean precipitation (figure 3(a)) and SDII (figure 3(b)). However, in some areas (small parts of KO, JP, and NEC, as well as the coastal part of YHR), internal variability remained the main contributor to total uncertainty for mean and SDII, while the areas of the internal uncertainty being the main contributor were more interspersed and larger for Rx5d and Rx1d (figures 4(c) and (d)). Scenario uncertainty accounted for an insignificant amount for the mean, but for the other indices, it started to show up in the southern part of Japan, the

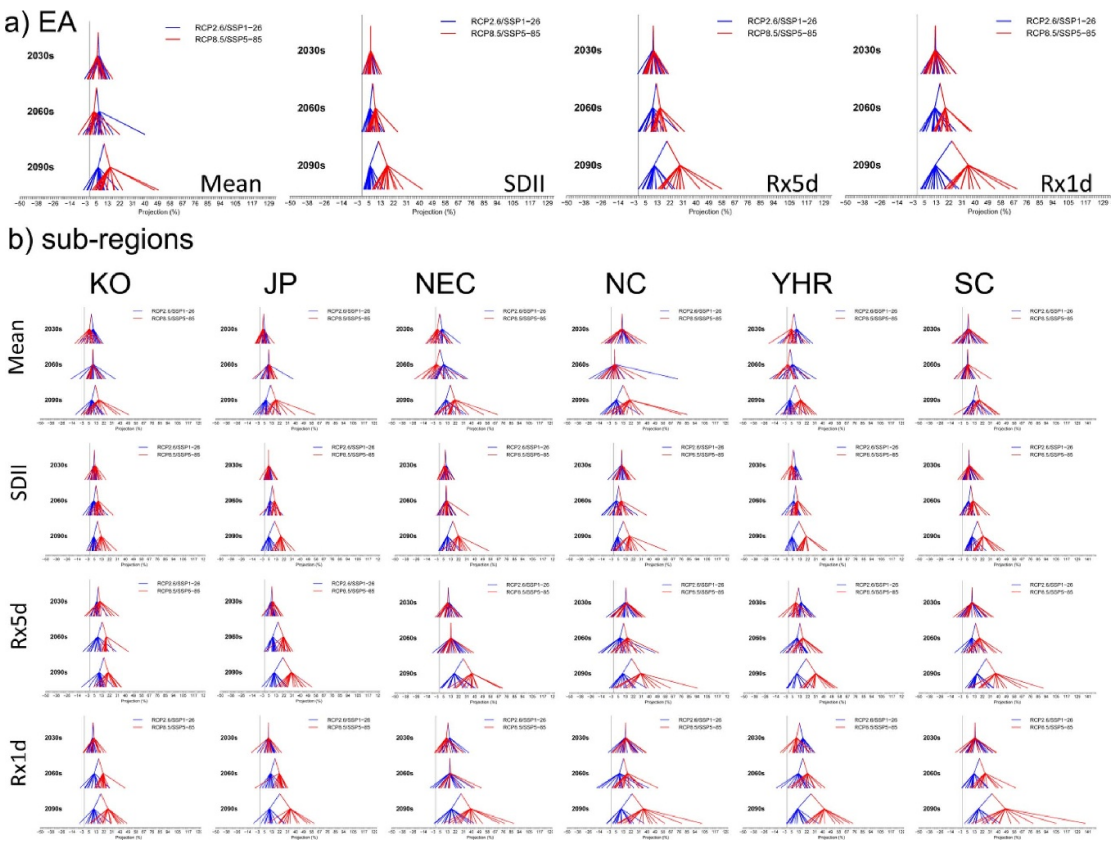

Figure 3. Cascade plots of the area-averaged predictions for (a) main domain, EA, and (b) each sub-region (left-to-rightKO, JP, NEC, NC, YHR, and SC, for the four indices (top-to-bottom: mean, SDII, Rx5d, and Rx1d). The point at the top is the mean change across all simulations, middle points are means across scenarios, and the bottom points show the change projected by each individual model. These points are connected with lines for figure readability. The simulations using RCP2.6/SSP1-2.6 scenarios are marked in blue, while the simulations with RCP8.5-SSP5-8.5 are marked in red. The graph shows three separate decades for each region: the 2030s, 2060s, and 2090s.

southwestern China, and the Russian *Primorsky Krai*. This indicates that extreme precipitation in these regions may become more sensitive to anthropogenic warming signals at an earlier period compared to other regions. Toward the end of the century (2090s), model uncertainty overall contributed to the largest portion of uncertainty for all indices. However, for SDII, Rx5d, and Rx1d there are parts of the domain where the scenario uncertainty accounts for more than 50% of the variability, namely in parts of JP, part of SC, and for Rx1d the southernmost part of KO. For mean precipitation, internal variability contribution was roughly double the scenario contribution at the end of the century, however for other indices, the contributions of scenario uncertainty and internal variability are overall comparable. Additionally, the contribution of the scenario uncertainty was larger for more extreme indices. This implies that extreme precipitation projections are more affected by different emissions and warming projections than the mean changes. The Russian *Primorsky Krai*, southern China, the southern region of KO, and JP were most affected by scenario uncertainty at the end of the century, while the northern part of KO, the northern part of JP and overall northwestern China were the least affected. This indicates that an enhanced anthropogenic warming signal is likely to have a greater impact on the projections of extreme precipitation indices in these regions.

All three uncertainty contributions to the total variance for the future projections averaged per region are shown in figure 5, for the primary domain and sub-regions. The influence of scenario uncertainty in each region at the end of the century tends to be greater for more extreme indices. For mean precipitation, scenario uncertainty accounted for between 13.2% (SC) and 29.2% (YHR) of the total uncertainty at the end of the century. For most regions, the contribution of scenario uncertainty is insignificant until the 2070s or 2080s. In contrast, for Rx1d, the scenario uncertainty during the last decade accounted for 37.2% (NEC) to 65.4% (JP) of the total. For Rx1d, JP was the most sensitive to emissions scenario differences, followed by

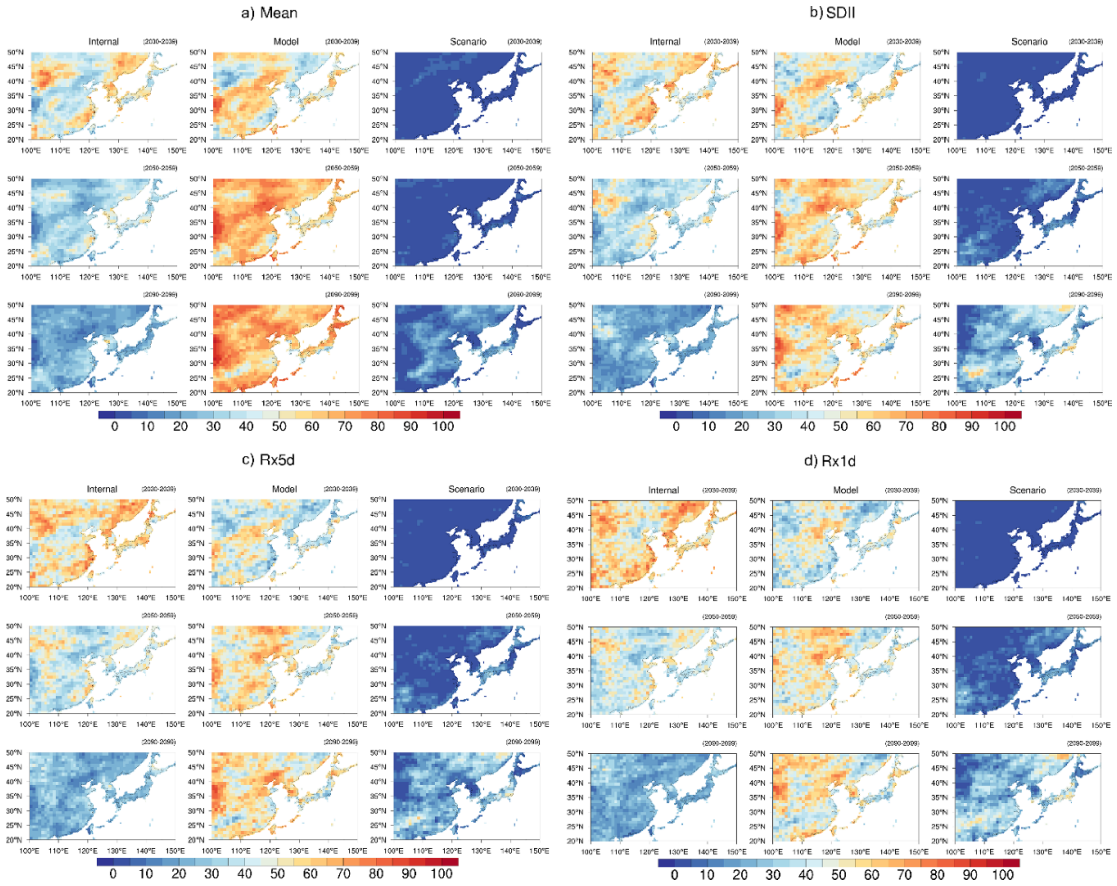

Figure 4. Individual uncertainty contributions [%] for (a) mean daily precipitation, (b) SDII, (c) Rx5d, and (d) Rx1d. The value shown in the figure is a decadal mean for the specified decade. In each sub-figure, the first, second, and third rows represent the 2030s, 2060s, and 2090s, respectively. The first, second, and third columns denote internal variability, model uncertainty, and scenario uncertainty, respectively.

YHR, and KO. The proportion of variability contributed by scenario uncertainty in most sub-regions is comparable for SDII, Rx5d, and Rx1d. Overall, model uncertainty was more influential in the drier regions (NC and NEC) for all of the indices, while internal variability had a higher influence, especially for extreme indices, in the wetter regions (KO, JP, and SC). The reason for the higher internal variability of the wetter regions could be attributed to the fact that they are affected by the EA summer monsoon (EASM), which is the largest contributor to annual precipitation in those regions. This contributes to internal variability and is also projected to strengthen in the future, leading to increased variability (Lee *et al* 2023).

Whilst the percentage contribution of each component provides an overall picture, it is also important to address the total uncertainty. Therefore, figure 6 shows the total uncertainty contributed by each component per region. The total amount of uncertainty, expressed in $\%^2$, was highest for Rx1d in all regions, reaching between $400\%^2$ in KO and $1000\%^2$ in SC by the end of the century, and the smallest for the SDII, between $100\%^2$ in KO and $240\%^2$ in NC. The uncertainty was overall the highest in NC and NEC, which most likely stems from these regions being relatively dry. This is because the percentile of uncertainty for relatively small amounts of change is high. Notably, however, at the end of the century, the highest uncertainty of Rx1d was recorded in the SC region. This result is due to a significant increase in scenario uncertainty at the end of the century in SC. Smaller sub-regions have more considerable internal variability than the whole domain, which is consistent with previous results (Hawkins and Sutton 2009, 2011, Park *et al* 2023). The internal variability for all indices was the highest in KO, the smallest among the sub-regions, which may have been considerably contributed by the influence of EASM. This is partially due to the fact that EASM itself is also connected to ENSO, which is part of internal variability. Therefore, areas where extreme precipitation

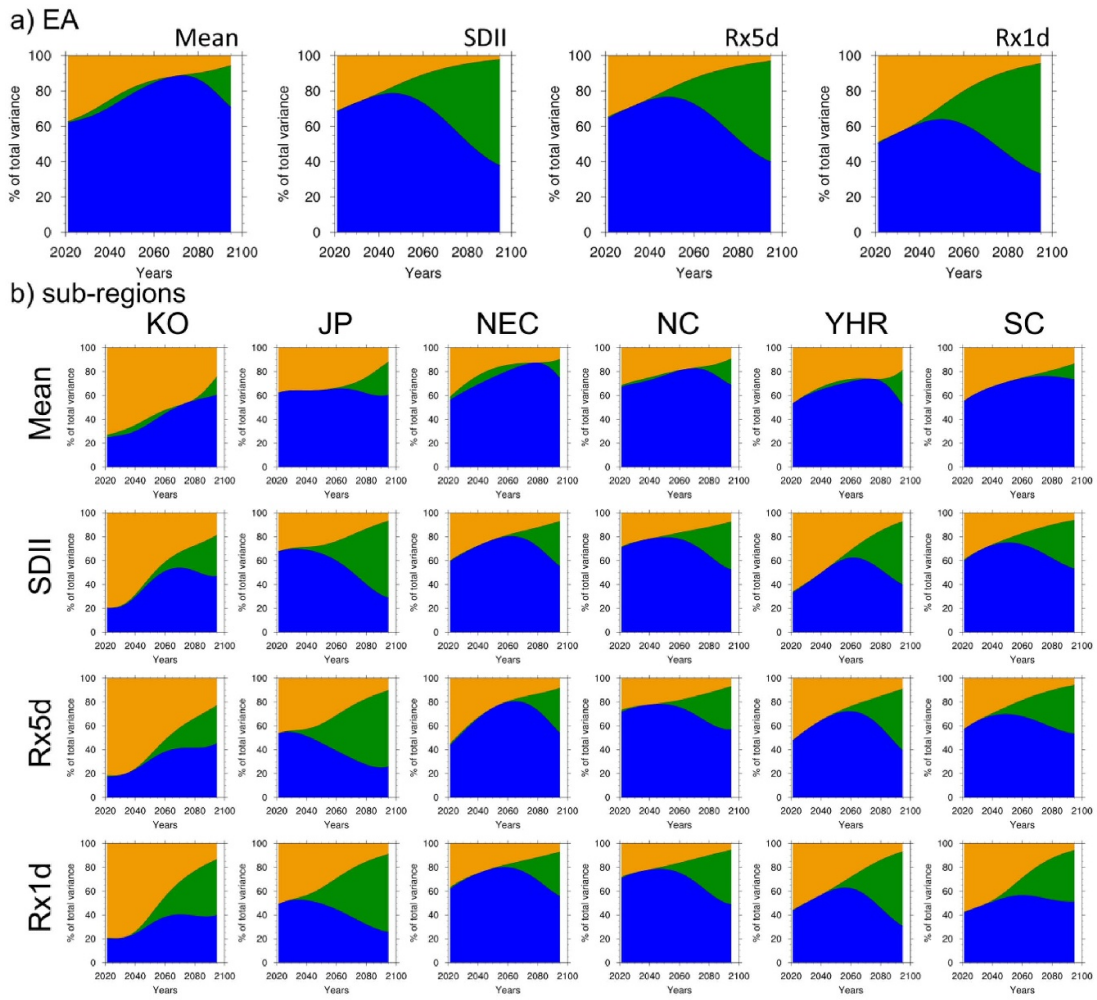

Figure 5. Individual uncertainty contributions for (a) the primary domain (EA), and (b) each sub-region (left-to-right: KO, JP, NEC, NC, YHR, and SC) for all four indices (top-to-bottom: Mean, SDII, Rx5d, and Rx1d). Model uncertainty is denoted in blue, scenario in green, and internal variability in orange.

is influenced more by EASM have higher internal variability. Additionally, the drier areas such as NEC and NC have higher model uncertainty because as the mean is smaller, the relative deviations from the mean due to model settings are higher. These results imply that since internal variability is a major source in near-term uncertainty in smaller regions. While the improvements in the near-term climate predictions might reduce internal variability somewhat (Cox and Stephenson 2007, Smith *et al* 2007, Hawkins and Sutton 2009, 2011, Park *et al* 2023), the internal variability is largely not significantly reducible as the effects of better initialization do not persist longer than few years (Hawkins *et al* 2016, Lehner and Dresen 2023). The model uncertainty for all indices was highest for the driest regions, that is, NC and NEC, for the same reason as the total uncertainty. For mean precipitation, scenario uncertainty was highest in NC at the end of the century and smallest in KO and SC. KO, JP, and NC regions all have a sudden uptick in the model uncertainty after 2085 for mean precipitation. For other indices, the increase in the model uncertainty is more gradual, except in the SC region for Rx1d. For the indices other than mean precipitation, the increase in total uncertainty was steeper after the 2060s in all regions, mainly contributable to the influence of the scenario uncertainty. Therefore, this means that warming caused by human activities will have a considerable impact on the increase in future extreme precipitation at the end of the century.

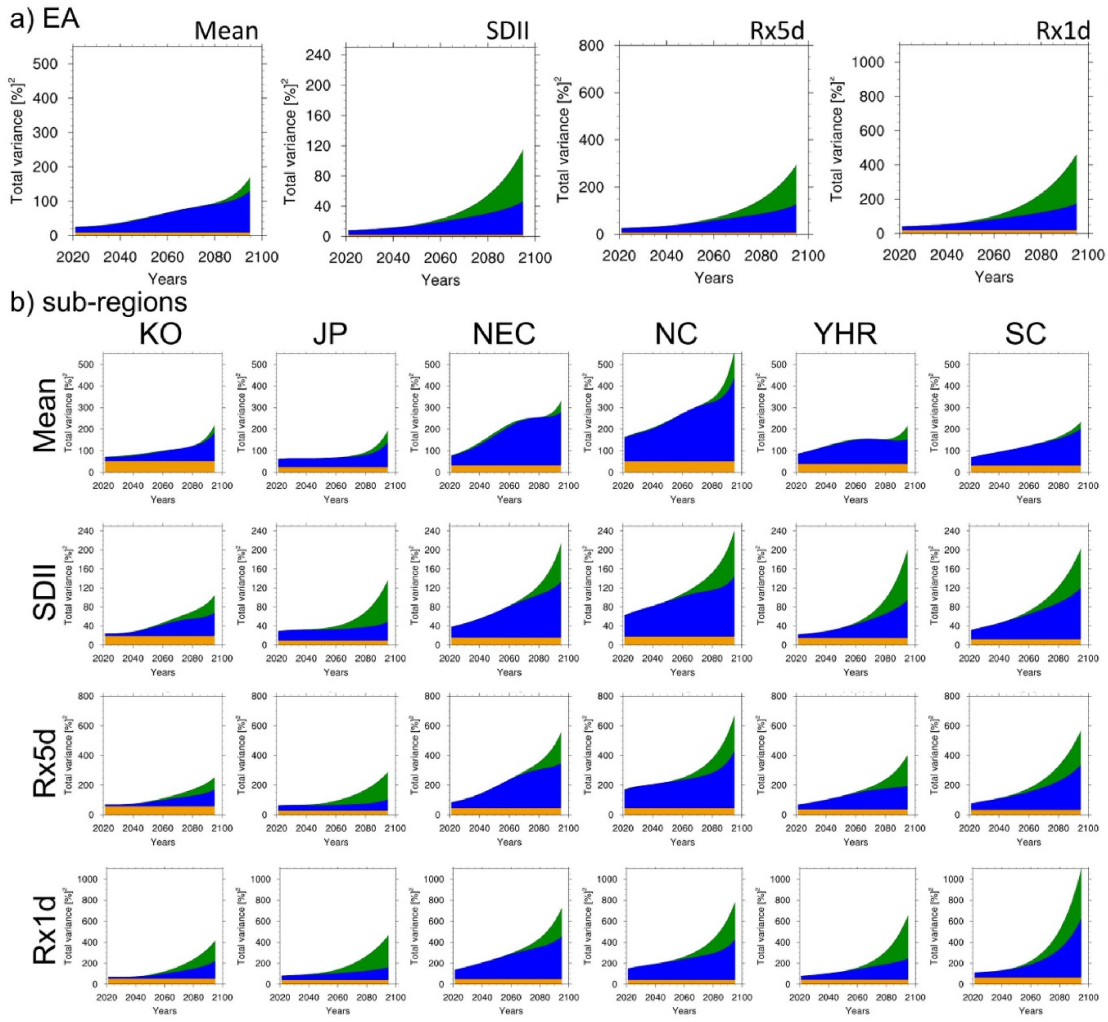

Figure 6. Total variance $[\%]^2$ attributable to individual uncertainties, for (a) the primary domain, and (b) each sub-region (left-to-right: KO, JP, NEC, NC, YHR, and SC) for all four indices (top-to-bottom: mean, SDII, Rx5d, and Rx1d). Model uncertainty is denoted in blue, scenario in green, and internal variability in orange. The *y*-axis ranges for the four indices are different from each other.

4. Conclusions and discussion

This study evaluated uncertainties in the predictions of the future precipitation extremes over the EA domain using multi-GCM–multi-RCM datasets at high resolution (25 km). In the low emissions scenarios, the projected changes in all indices were stable, with a mild increase until the mid-future period, followed by a slight decrease toward the end of the century. However, in the high-emissions scenarios, there was a continuous increase until the end of the century, which was more prominent with more extreme indices. That is, the largest increase (>50% in some regions of the domain) was projected for Rx1d, which is consistent with previous studies (Kim *et al* 2018, Park *et al* 2021).

Different component contributions to the uncertainty were quantitatively assessed. Overall, at the beginning of the century, the model uncertainty accounted for the majority of the uncertainty in most sub-regions for most indices, with the exception of KO, where internal variability accounted for the largest part of the uncertainty (figure 5). As the internal variability is not time dependent, and the model and scenario uncertainty increase in time, the contribution of the internal variability got lower further in the future.

Scenario uncertainty played an insignificant role in most of the domains for all periods in the mean precipitation projections. However, for more extreme indices, the scenario uncertainty contributed to a larger proportion of the uncertainty, with its influence starting somewhat earlier for KO and JP than other domains. By the end of the century, the influence of the scenario uncertainty surpassed internal variability for all sub-regions, as well as model uncertainty in some sub-regions (KO, JP, and YHR; figure 5), for all extreme precipitation indices. As the model spread is partially dependent on the climate sensitivity of the models (Effective Climate Sensitivity (EffCs), e.g. Schlund *et al* 2020, Meehl *et al* 2020), a more in-depth study on the reasons for the model spread, and the

effect of different factors, including EffCS and aerosol impacts is planned to be conducted in the future. The figures showing the relationship between the EffCS of the GCMs used in this study and the change in precipitation indices for the three periods, and both scenarios used in this study are included in the supplementary files, along with the table noting all of the values.

Conversely, the influence of different sources of uncertainty is not equally distributed all over the specific sub- regions. Namely, the northern part of the KO region displayed a fairly low scenario uncertainty for all of the indices even at the end of the century; however, in the southern part, for Rx1d, scenario uncertainty exceeded 50% in some parts. A similar pattern was observed in Japan, with the central and southern regions being more affected by scenario uncertainty with some areas having scenario uncertainty as the main contributor (>50%) by the end of the century (figure 4).

In conclusion, in some parts of EA, changes in extreme precipitation are largely dependent on emissions. The areas that experience the heaviest precipitation under the current climate (KO, JP, SC, and YHR) also have the highest contribution from scenario uncertainty. The significance of this study lies in the demonstrated differences in the factors that affect the mean (usually analyzed) and extreme uncertainties. Specifically, we demonstrated that scenario uncertainty plays a greater role in the projections of the extreme precipitation than the mean despite more total variance. Therefore, there are several potential uses for this study. First, as the results of the simulations of the extremes are often used in impact studies, such as calculating the return values of precipitation for the purpose of flood defense systems, the impact modelers could benefit from the findings of this study. Namely, being aware that extreme projections are inherently more uncertain than the projections of means, therefore data should be used with caution. Especially in the short term, where internal variability plays a high role in some regions, impact modelers should take this into account when modeling the impact and suggesting potential responses. Additionally, the results of this study could be used as a reference for the stakeholders and policymakers, emphasizing the need for low-emission policies to prevent potentially catastrophic disasters caused by extreme precipitation events, as scenario uncertainty plays a heightened role at the end of the century.

The results in the present study are only partially consistent with those of Xu *et al* (2019), which showed that for extreme precipitation over China, the influence of the model is higher than that of the scenario. However, as the method used was different, and the internal variability was not accounted for at all, in the aforementioned study larger amount of variability (>90%) comes from models, rather than scenarios, while the present study showed that the scenario influence is not insignificant, especially at the end of the century. In addition, our results are also in agreement with those of both Zhou *et al* (2014) and Zhou *et al* (2020), who concluded that scenario uncertainty plays a greater role in extreme precipitation than it does for means. The internal variability comes from two sources: the natural variability of the earth's climate systems and the variability in the model calculations. It is assumed that progress in our understanding of climate systems and improvements in near-term climate predictions will result in the reduction of internal variability in the near-future (Cox and Stephenson 2007, Smith *et al* 2007, Hawkins and Sutton 2009, 2011, Park *et al* 2023).

This study has a limitation related to the data used: the number of models was relatively small, only two scenario combinations were used, and only one run of each model was used. In particular, for CMIP6, only one forcing GCM was used, namely, the UKESM, which has a relatively high climate sensitivity. It would be interesting to repeat this study once more GCM–RCM combinations become available, and more runs of the same models are conducted. Additionally, one further limitation of the current study lies in the design of RCM experiments. As they are climate models and not Earth System Models, aerosol interactions, land use, biology, and even air-sea coupling were not included, and the future scenario forcing only included changes in greenhouse gases. This limitation will be addressed in the future through the development of a regional earth system model.

We also have a future plan to analyze the uncertainties for the mean and extreme values of different variables such as temperature and relative humidity. In particular, we will focus on the uncertainties of temperature-related extreme events, because EA is the domain in which both precipitation and temperature extremes tend to occur in the same season (boreal summer).

Data availability statement

The data that support the findings of this study are openly available at the following URL/DOI: https://esg-dn1.nsc.liu.se/search/cordex/.

Acknowledgments

This work was funded by the Korea Meteorological Administration Research and Development Program under Grant KMI (RS-2024-00403386). The model simulations were performed by using the supercomputing resource of the Korea Meteorological Administration (National Center for Meteorological Supercomputer).

ORCID iDs

Ana Juzbašić https://orcid.org/0000-0002-3820-790X
Dong-Hyun Cha https://orcid.org/0000-0001-5053-6741
Joong-Bae Ahn https://orcid.org/0000-0001-6958-2801
Eun-Chul Chang https://orcid.org/0000-0002-5784-447X
Seung-Ki Min https://orcid.org/0000-0002-6749-010X

References

Andrews T, Ringer M A, Doutriaux-Boucher M, Webb M J and Collins W J 2012 Sensitivity of an Earth system climate model to idealized radiative forcing *Geophys. Res. Lett.* **39** 10

Chen H P, Sun J Q and Chen X L 2014 Projection and uncertainty analysis of global precipitation-related extremes using CMIP5 models *Int. J. Climatol.* **34** 2730–48

Christensen O B and Kjellström E 2021 Filling the matrix: an ANOVA-based method to emulate regional climate model simulations for equally-weighted properties of ensembles of opportunity *Clim. Dyn.* **58** 2371–85

Cox P and Stephenson D 2007 A changing climate for prediction *Science* **317** 207–8

Davies T, Cullen M J P, Malcolm A J, Mawson M H, Staniforth A, White A A and Wood N 2005 A new dynamical core for the met office's global and regional modelling of the atmosphere *Q. J. R. Meteorol. Soc.* **131** 1759–82

Doms G and Baldauf M 2013 A description of the nonhydrostatic regional COSMO-model *Part I: Dynamics and Numerics, Tech. Rep.* (COSMO—Consortium for Small- Scale Modelling) (https://doi.org/10.5676/DWD_pub/nwv/cosmo-doc_5.00_I)

Flato G *et al* 2013 Evaluation of climate models *Climate Change 2013: The Physical Science Basis* (Contribution of Working Group I to the Fifth Assessment Report of the Intergovernmental Panel on Climate Change) (https://doi.org/10.1038/srep02645)

Gao X, Xu Y, Zhao Z, Pal J S and Giorgi F 2006 On the role of resolution and topography in the simulation of East Asia precipitation *Theor. Appl. Climatol.* **86** 173–85

Giorgetta M A *et al* 2013 Climate and carbon cycle changes from 1850 to 2100 in MPI-ESM simulations for the coupled model intercomparison project phase 5 *J. Adv. Model. Earth Syst.* **5** 572–97

Giorgi F *et al* 2012 RegCM4: model description and preliminary tests over multiple CORDEX domains *Clim. Res.* **52** 7–29

Gochis D J *et al* 2017 The weather research and forecasting model: overview, system efforts, and future directions *Bull. Am. Meteorol. Soc.* **98** 1717–37

Grell G A, Dudhia J and Stauffer D 1994 A description of the fifth-generation Penn State/NCAR mesoscale model (MM5) (University Corporation for Atmospheric Research) (https://doi.org/10.5065/D60Z716B)

Guo Y, Cao J, Li H, Wang J and Ding Y 2016 Simulation of the interface between the Indian summer monsoon and the East Asian summer monsoon: intercomparison between MPI-ESM and ECHAM5/MPI-OM *Adv. Atmos. Sci.* **33** 294–308

Hawkins E 2014 *Climate Lab Book* (available at: www.climate-lab-book.ac.uk/2014/cascade-of-uncertainty)

Hawkins E, Smith R S, Gregory J M and Stainforth D A 2016 Irreducible uncertainty in near-term climate projections *Clim. Dyn.* **46** 3807–19

Hawkins E and Sutton R 2009 The potential to narrow uncertainty in regional climate predictions *Bull. Am. Meteorol. Soc.* **90** 1095–108

Hawkins E and Sutton R 2011 The potential to narrow uncertainty in projections of regional precipitation change *Clim. Dyn.* **37** 407–18

Hong S-Y *et al* 2013 The global/regional integrated model system (GRIMs) *Asia-Pac. J. Atmos. Sci.* **49** 219–43

Hui P, Wei F, Xiao Y, Yang J, Xu J and Tang J 2022 Future projection of extreme precipitation within CORDEX East Asia phase II: multi-model ensemble *Theor. Appl. Climatol.* **150** 1271–93

IPCC 2014 Climate change 2014: impacts, adaptation, and vulnerability *Part A: Global and Sectoral Aspects* (*Contribution of Working Group II to the Fifth Assessment Report of the Intergovernmental Panel on Climate Change*)

IPCC 2022 Climate change 2022: impacts, adaptation, and vulnerability *Contribution of Working Group II to the Sixth Assessment Report of the Intergovernmental Panel on Climate Change*

Jo S, Ahn J-B, Cha D-H, Min S-K, Suh M-S, Byun Y-H and Kim J-U 2019 The koppen-trewartha climate-type changes over the CORDEX-East Asia phase 2 domain under 2 and 3 degrees C global warming *Geophys. Res. Lett.* **46** 14030–41

Juzbašić A, Ahn J-B, Cha D-H, Chang E-C and Min S-K 2022 Changes in heat stress considering temperature, humidity, and wind over East Asia under RCP8.5 and SSP5-8.5 scenarios *Int. J. Climatol.* **42** 6579–95

Kim G *et al* 2018 Future change in extreme precipitation indices over Korea *Int. J. Climatol.* **38** e862–e874

Kim G *et al* 2020a Evaluation and projection of regional climate over East Asia in CORDEX-East Asia phase I experiment *Asia-Pac. J. Atmos. Sci.* **57** 119–34

Kim G, Kim J and Cha D-H 2022 Added value of high-resolution regional climate model in simulating precipitation based on the changes in kinetic energy *Geosci. Lett.* **9** 38

Kim J, Kim T, Kim D-H, Kim J-W, Cha D-H, Min S-K and Kim Y-H 2020b Evaluation of performance and uncertainty for multi-RCM over CORDEX-East Asia phase 2 region *Atmosphere* **30** 376 (in Korean with English abstract)

Kim Y-H, Ahn J-B, Suh M-S, Cha D-H, Chang E-C, Min S-K, Byun Y-H and Kim J-U 2023 Future changes in extreme heatwaves in terms of intensity and duration over the CORDEX-East Asia phase two domain using multi-GCM and multi-RCM chains *Environ. Res. Lett.* **18** 034007

Klein Tank A M G, Zwiers F W and Zhang X 2009 Guidelines on analysis of extremes in a changing climate in support of informed decisions for adaptation *Climate Data and Monitoring Rep* WCDMP 72, WMO-TD 1500 p 56

Kutiel H 2019 Climatic uncertainty in the mediterranean basin and its possible relevance to important economic sectors *Atmosphere* **10** 10

Lafferty D C and Sriver R L 2023 Downscaling and bias-correction contribute considerable uncertainty to local climate projections in CMIP6 *npj Clim. Atmos. Sci.* **6** 158

Lee D, Min S-K, Ahn J-B, Cha D-H, Shin S-W, Chang E-C, Suh M-S, Byun Y-H and Kim J-U 2023 Uncertainty analysis of future summer monsoon duration and area over East Asia using a multi-GCM/multi-RCM ensemble *Environ. Res. Lett.* **18** 064026

Lee D, Min S-K, Jin J, Lee J-W, Cha D-H, Suh M-S, Ahn J-B, Hong S-Y, Kang H-S and Joh M 2017 Thermodynamic and dynamic contributions to future changes in summer precipitation over Northeast Asia and Korea: a multi-RCM study *Clim. Dyn.* **49** 4121–39

Lee J-Y *et al* 2021 Future global climate: scenario-based projections and near-term information *Climate Change 2021: The Physical Science Basis* (Contribution of Working Group I to the Sixth Assessment Report of the Intergovernmental Panel on Climate Change) (https://doi.org/10.1017/9781009157896.006)

Lehner F, Deser C, Maher N, Marotzke J, Fischer E M, Brunner L, Knutti R and Hawkins E 2020 Partitioning climate projection uncertainty with multiple large ensembles and CMIP5/6 *Earth Syst. Dyn.* **11** 491–508

Lehner F and Dresen C 2023 Origin, importance, and predictive limits of internal climate variability *Environ. Res. Clim.* **2** 023001

Li J J, Huo R, Chen H, Zhao Y and Zhao T H 2021 Comparative assessment and future prediction using CMIP6 and CMIP5 for annual precipitation and extreme precipitation simulation *Front. Earth Sci.* **9** 687976

Lock A P, Brown A R, Bush M R, Martin G M and Smith R N B 2000 A new boundary layer mixing scheme. Part I: scheme description and single-column model tests *Mon. Weather Rev.* **128** 3187–99

Martin G M *et al* 2011 The HadGEM2 family of met office unified model climate configurations *Geosci. Model Dev.* **4** 723–57

Meehl G A, Senior C A, Eyring V, Flato G, Lamarque J-F, Stouffer R J, Taylor K E and Schlund M 2020 Context for interpreting equilibrium climate sensitivity and transient climate response from the CMIP6 Earth system models *Sci. Adv.* **6** eaba1981

Monier E, Gao X, Scott J R, Sokolov A P and Schlosser C A 2014 A framework for modeling uncertainty in regional climate change *Clim. Change* **131** 51–66

Park C *et al* 2016 Evaluation of multiple regional climate models for summer climate extremes over East Asia *Clim. Dyn.* **46** 2469–86

Park C *et al* 2023 Uncertainty assessment of future climate change using bias–corrected high–resolution multi–regional climate model datasets over East Asia *Clim. Dyn.* **62** 1983–96

Park C, Cha D-H, Kim G, Lee G, Lee D-K, Suh M-S, Hong S-Y, Ahn J-B and Min S-K 2020 Evaluation of summer precipitation over Far East Asia and South Korea simulated by multiple regional climate models *Int. J. Climatol.* **40** 2270–84

Park C, Lee G, Kim G and Cha D-H 2021 Future changes in precipitation for identified sub-regions in East Asia using bias-corrected multi-RCMs *Int. J. Climatol.* **41** 1889–904

Rajczak J, Pall P and Schär C 2013 Projections of extreme precipitation events in regional climate simulations for Europe and the Alpine Region *J. Geophys. Res. Atmos.* **118** 3610–26

Rummukainen M 2015 Added value in regional climate modeling *WIREs Clim. Change* **7** 145–59

Samset B H, Lund M T, Bollasina M, Myhre G and Wilcox L 2019 Emerging Asian aerosol patterns *Nat. Geosci.* **12** 582–4

Schlund M, Lauer A, Gentine P, Sherwood S C and Eyring V 2020 Emergent constraints on equilibrium climate sensitivity in CMIP5: do they hold for CMIP6? *Earth Syst. Dyn.* **11** 1233–58

Sellar A A *et al* 2019 UKESM1: description and evaluation of the U.K. Earth system model *J. Adv. Model. Earth Syst.* **11** 4513–58

Seo G-Y, Ahn J-B, Cha D-H, Suh M-S, Min S-K, Chang E-C, Byun Y-H and Kim J-U 2023 Evaluation of multi-RCM ensembles for simulating spatiotemporal variability of Asian summer monsoon precipitation in the CORDEX-East Asia Phase 2 domain *Int. J. Climatol.* **43** 3710–29

Seo K-H, Ok J, Son J-H and Cha D-H 2013 Assessing future changes in the East Asian summer monsoon using CMIP5 coupled models *J. Clim.* **26** 7662–75

Smith D M, Cusack S, Colman A W, Folland C K, Harris G R and Murphy J M 2007 Improved surface temperature prediction for the coming decade from a global climate model *Science* **317** 796–9

Smith R N B 1990 A scheme for predicting layer clouds and their water content in a general circulation model *Q. J. R. Meteorol. Soc.* **116** 435–60

Suzuki-Parker A, Kusaka H, Takayabu I, Dairaku K, Ishizaki N N and Ham S 2018 Contributions of GCM/RCM uncertainty in ensemble dynamical downscaling for precipitation in East Asian summer monsoon season *Sola* **14** 97–104

Swart N C, Fyfe J C, Hawkins E, Kay J E and Jahn A 2015 Influence of internal variability on Arctic sea-ice trends *Nat. Clim. Change* **5** 86–89

Torma C, Giorgi F and Coppola E 2015 Added value of regional climate modeling over areas characterized by complex terrain—precipitation over the Alps *JGR Atmos.* **120** 3957–72

Vial J, Dufresne J L and Bony S 2013 On the interpretation of inter-model spread in CMIP5 climate sensitivity estimates *Clim. Dyn.* **41** 3339–62

Wilcox L J *et al* 2020 Accelerated increases in global and Asian summer monsoon precipitation from future aerosol reductions *Atmos. Chem. Phys.* **20** 11955–77

Xu K, Xu B B, Ju J L, Wu C H, Dai H and Hu B X 2019 Projection and uncertainty of precipitation extremes in the CMIP5 multimodel ensembles over nine major basins in China *Atmos. Res.* **226** 122–37

Zadeh N *et al* 2012 GFDL's ESM2 global coupled climate– carbon Earth system models. Part I: physical formulation and baseline simulation characteristics *J. Clim.* **25** 6646–65

Zhao A D, Stevenson D S and Bollasina M A 2019 The role of anthropogenic aerosols in future precipitation extremes over the Asian monsoon region *Clim. Dyn.* **52** 6257–78

Zhou B, Wen Q H, Xu Y, Song L and Zhang X 2014 Projected changes in temperature and precipitation extremes in China by the CMIP5 multimodel ensembles *J. Clim.* **27** 6591–611

Zhou T, Lu J, Zhang W and Chen Z 2020 The sources of uncertainty in the projection of global land monsoon precipitation *Geophys. Res. Lett.* **47** e2020GL088415